NANO LETTERS

pubs.acs.org/NanoLett Letter

Metasurfaces with Planar Chiral Meta-Atoms for Spin Light Manipulation

Chen Chen, Shenglun Gao, Wange Song, Hanmeng Li, Shi-Ning Zhu, and Tao Li*

Cite This: https://dx.doi.org/10.1021/acs.nanolett.0c04902 Read Online

ACCESS | Metrics & More | Article Recommendations | Supporting Information

ABSTRACT: Spin light (i.e., circularly polarized light) manipulation based on metasurfaces with a controlled geometric phase (i.e., Pancharatnam–Berry (PB) phase) has achieved great successes according to its convenient design and robust performances, by which the phase control is mainly determined by the rotation angle of each meta-atom. This PB phase can be regarded as a global effect for spin light; here, we propose a local phase manipulation for metasurfaces with planar chiral meta-atoms. Planar chiral meta-atoms break fundamental symmetry restrictions and do not need a rotation for these kinds of meta-atoms to manipulate the spin light, which significantly expands the functionality of metasurface as it is incorporated with other modulations (e.g., PB phase, propagation phase). As an example, spin-decoupled holographic imaging is demonstrated with robust and broadband properties. Our work definitely enriches the design of metasurfaces and may trigger more exciting chiral-optics applications.

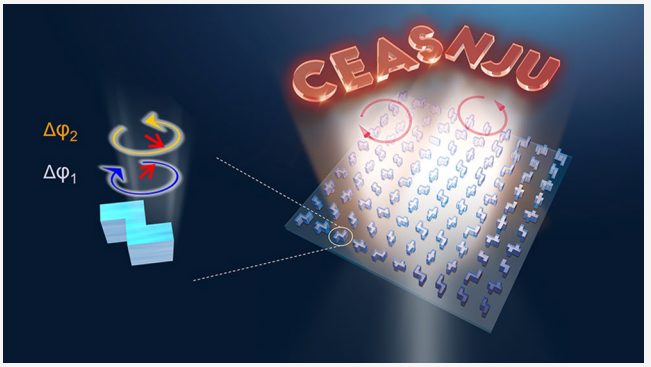

KEYWORDS: *Dielectric metasurfaces, spin decoupling, chiral meta-atoms, meta-hologram*

Metasurfaces, composed of subwavelength artificial atoms, possess unprecedented ability to manipulate the amplitude, phase, polarization, and spectral response of the light.[1−3] Versatile fascinating functionalities have been demonstrated, such as metalens,[4−6] meta-holograms,[7−9] waveplates,[10,11] etc. They were implemented by flexible meta-atom designs based on wavelength-dependent resonances,[1,12−14] a circular polarization-dependent PB phase,[15] and a high nanopost-induced dynamic phase (i.e., propagation phase)[16] both in metallic and all-dielectric metasurfaces. Since each method has its advantages and disadvantages,[17] they are developing a path to work in joint manipulations for implementation of complex functions and better performances.[15,18−21]

As for circularly polarized (CP) light, PB phase with the capability of achieving a full phase control by arranging the orientation angle (θ) of the anisotropic antennas (acting as half waveplates) is the most popular method to realize the wave manipulation for its convenience and relative robustness against the antennas size and roughness. However, there are fundamental symmetry restrictions between two CP light phases, resulting in limited functions. For example, if a focusing phase profile is designed with respect to RCP light, it turns to divergent for the LCP light. Considerable efforts have been devoted to break the symmetry and realize the spin-decoupled functions, including interleaved meta-atoms both based on PB phase,[22−28] the combination of PB phase with dynamic phase,[15,19,29−] and others.[37−40]

In this work, we develop a new route for the phase manipulation of metasurfaces based on the C2-symmetric nanoantennas (so-called chiral meta-atoms), based on which two orthogonal CP light phases can be modulated independently. Different holograms are presented in high performances as the spin switched. In addition, these chiral meta-atoms could also be collaborated with PB phase, which provides more possibilities for chiral applications. This engineering of chiral meta-atoms promises the full potential for spin light manipulations and suggests new optical devices and applications.

The current construction of metasurface in visible or near-infrared regions is usually composed of anisotropic nanorods. Under linearly polarized (along with one of its axes) illuminations, only the induced current (conductive current in metal meta-atoms or displacement current in dielectric meta-atoms) in the same direction can be excited due to the intrinsic mirror symmetry, as the schematics show in Figure 1(a), where the red arrows represent the induced current. Thus, there is no phase shift for CP light, which is only

Received: December 14, 2020
Revised: January 27, 2021

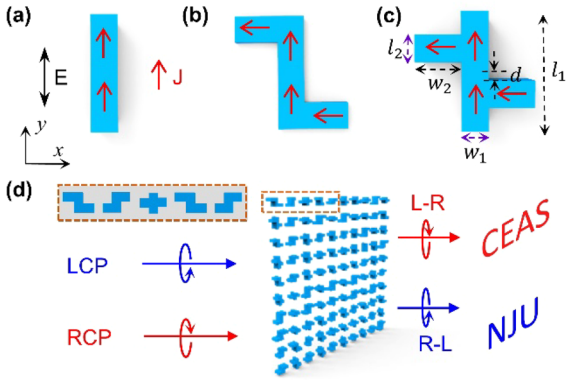

Figure 1. Illustration of chiral meta-atoms for wave manipulation. Schematics of (a) a planar meta-atom with mirror symmetry, (b) a Z-shaped meta-atom which breaks mirror symmetry and n-fold ($n > 2$) rotational symmetry (i.e., chiral meta-atom), and (c) a general Z-shaped meta-atom for more structural degrees. Parameters marked in black are variables, while the ones in purple remain unchanged. The red arrows in (a–c) mark the direction of the current flow excited by y-polarized electric field. (d) Schematics of a metasurface made of chiral meta-atoms without rotation for spin-decoupled hologram, where two irrelative holographic images are displayed according to different CP illuminations.

achieved by rotating the meta-atoms for the phase control (i.e., PB phase). On the contrary, if the mirror symmetry and n-fold ($n > 2$) rotational symmetries[41] of the meta-atom are broken (e.g., Z-shaped meta-atom, see Figure 1(b)), then the current in the orthogonal direction will come into play and would lead to a phase shift for different CP light. Thus, there is no need of rotation for these kinds of meta-atoms to manipulate the spin light.

Normally, a planar anisotropic dielectric meta-atom with subwavelength height can be modeled as an electric dipole in the x–y plane. Considering the illumination of CP light, its radiation electric field E in a reflection/transmission way becomes (detailed derivation can be found in Supporting Information Sec. I):

$$E = \begin{cases} A_0(A_1 e^{i\theta_1}\vec{s_+} + A_2 e^{i\theta_2}\vec{s_-}), \text{ where } \sigma = 1 \\ A_0(A_2 e^{-i\theta_2}\vec{s_+} + A_1 e^{-i\theta_1}\vec{s_-}), \text{ where } \sigma = -1 \end{cases} \quad (1)$$

where $A_0 = \frac{-\omega^2}{4\pi\varepsilon_0 c^2 R} e^{ikR}$, $\theta_1 = \arctan\frac{\alpha_{xy} - \alpha_{yx}}{\alpha_{xx} + \alpha_{yy}}$, $\theta_2 = \arctan\frac{\alpha_{xy} + \alpha_{yx}}{\alpha_{xx} - \alpha_{yy}}$, $A_1 = \frac{1}{2}\sqrt{(\alpha_{xx} + \alpha_{yy})^2 + (\alpha_{xy} - \alpha_{yx})^2}$, $A_2 = \frac{1}{2}\sqrt{(\alpha_{xx} - \alpha_{yy})^2 + (\alpha_{xy} + \alpha_{yx})^2}$. The variables α_{xx}, α_{xy}, α_{yx}, and α_{yy} are the corresponding components of the electric polarizability tensor. The variable $\sigma = \pm 1$ represents the incident RCP and LCP. The variables $\boldsymbol{s}_+$ and $\boldsymbol{s}_-$ are the unit vectors of the circularly polarized light when the incidence is perpendicular to the x–y plane. R is the distance from the dipole, c is the light speed in vacuum, ε_0 is the permittivity in vacuum, and ω is the frequency of the light.

For meta-atoms that satisfy planar mirror or n-fold ($n > 2$) rotational symmetries, as a nanorod shown in Figure 1(a), their cross components α_{xy} & $\alpha_{yx} = 0$, and there is no phase delay difference between the incident CP light and its orthogonal polarization state. However, for a chiral meta-atom, there comes α_{xy} & $\alpha_{yx} \neq 0$, and the phase delays of the cross-CP light with different CP light incidence diversify. As shown in eq 1, when the handedness is switched, the phase shifts of the transmitted and converted CP light are reversed accordingly. It is further confirmed by simulations of the corresponding periodic meta-atoms based on silicon at the wavelength of 980 nm using Lumerical software (see Supporting Information Sec. II for details). The influence of meta-atoms symmetry on phase shifts for different CP light is well demonstrated, as the simulation results are shown in Figure S1.

To fully investigate the phase delays of the chiral meta-atom, we generalized the Z-shaped meta-atom model with multiple structural parameters (labeled in Figure 1(c)). This provides us with wide parameter spaces to achieve flexible control of the light field. Here, key parameters marked in black, i.e., l_1, w_2, and d, are variables, corresponding to the length of the middle rod, the arm length on each side, and the spacing between

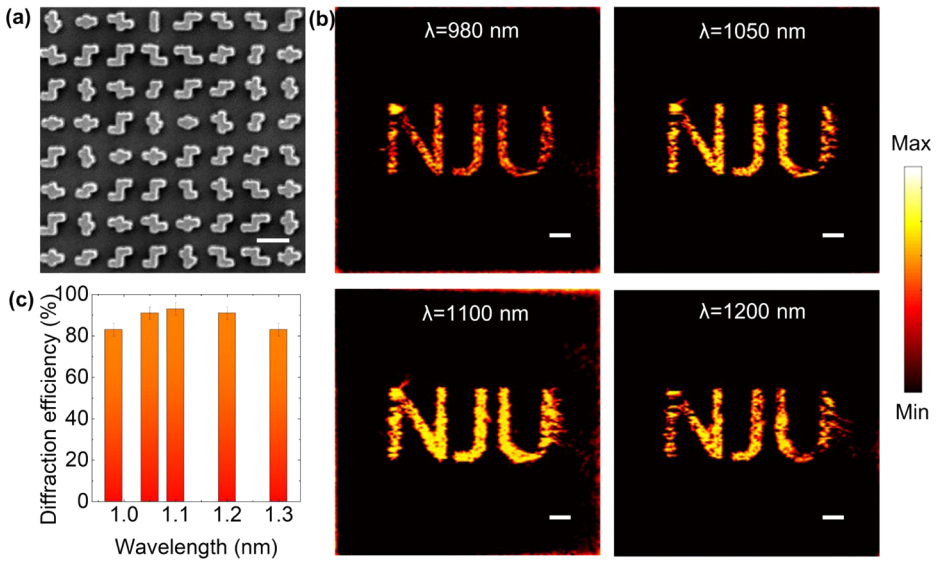

Figure 2. (a) SEM micrograph of the metasurface composed of chiral meta-atoms for hologram imaging. Scale bar: 500 nm. Measured hologram imaging (without cross-polarization analysis) with RCP incidence at the wavelengths of (b) 980, 1050, 1100, and 1200 nm. Scale bar: 20 μm. (c) Measured diffraction efficiency at different wavelengths.

https://dx.doi.org/10.1021/acs.nanolett.0c04902
Nano Lett. XXXX, XXX, XXX–XXX

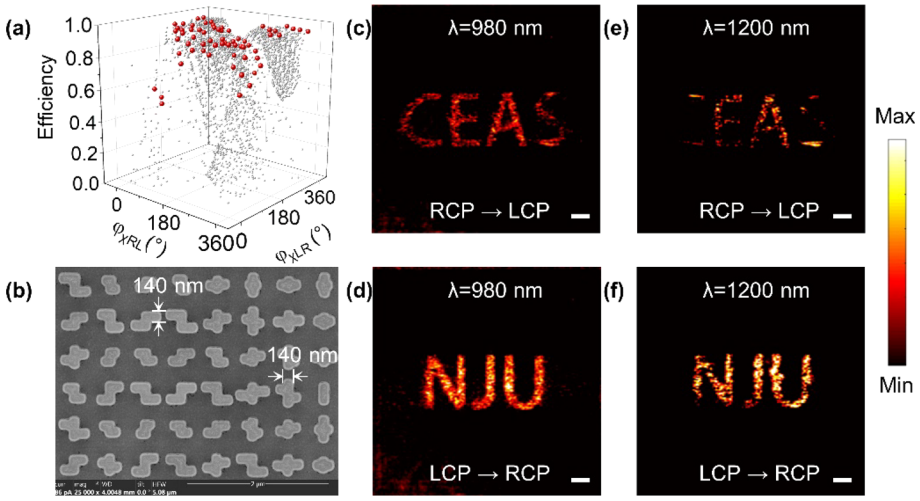

Figure 3. Spin-decoupled holograms with chiral meta-atoms. (a) Simulated diffraction efficiency distribution with selected meta-atoms marked in red. (b) SEM micrograph of the metasurface. Scale bar is 2 μm. Experimental results with (c) RCP incidence and (d) LCP incidence without analyzers, and corresponding results (e, f) at λ = 1200 nm. Scale bar is 20 μm.

them. Other parameters marked in purple (w_1, l_2) keep fixed for the unification of the feature size in the fabrication process. Arranging different chiral meta-atoms in suitable positions enables sophisticated wavefront manipulation. Figure 1(d) illustrates the schematic of spin-decoupled hologram imaging based on chiral meta-atoms (marked in a yellow dotted box) in a transmission way.

The efficiencies and phase retardation of different chiral meta-atoms are obtained by full-wave simulations. The meta-atom material is amorphous silicon with the height (h) of 800 nm, and the substrate is fused silica. The wavelength of CP light (λ) is chosen as 980 nm. The unit cell period is set as 500 nm to meet the Nyquist sampling criterion[42] to avoid the unwanted diffraction orders. This kind of meta-atom satisfies C_2 symmetry. The variables w_1 and l_2 in Figure 1(c) are set as 80 nm. Figures S2(a−c) display the diffraction efficiency (converted CP light/total transmitted light) distribution in the parameter space which consisted of w_2 and l_1 when d = −40, 0, and 40 nm. Meta-atoms with high conversion efficiency account for a large proportion. The corresponding phase delay distributions are shown in Figures 2S(d−f), which is sufficient to achieve full phase control.

For a basic demonstration of phase modulation capability by such kind of chiral meta-atoms, a meta-hologram was designed to generate an image of "NJU" (abbreviation of Nanjing University) at a 100 μm distance, which was successfully obtained in experiments. The phase profiles yielding the hologram image is computed using Gerchberg−Saxton iterative phase retrieval.[43,44] To obtain precise phase control, 36 different meta-atoms were selected to cover the 2π phase range, and all the selected unit elements are listed in Table S1. The scanning electron microscopy (SEM) image of the fabricated sample (D = 250 μm) is shown in Figure 2(a), consisting of different Z-shaped meta-atoms (sample fabrication can be seen in Supporting Information Sec. IV). The sample is illuminated by a laser beam with a wavelength of 980 nm. A linear polarizer (LP) and a quarter-wave plate (QWP) are utilized to generate CP incidence. A near-infrared (NIR) camera (Xeva-1.7-320) is employed to capture the light intensity profile through a microscope objective. The measured hologram image at λ = 980 nm is displayed in Figure 2(b), clearly showing the letters "NJU". Given the mismatch between the designed and the fabricated meta-atom sizes (~30 nm deviations, the detailed measurement can be seen in Figure S5), this indicates the robustness of the proposed phase modulation. Moreover, the chiral meta-atom design is also considerably insensitive to the working wavelengths that indicates a broadband property (see Figure 2(b)). This phase modulation depends on the charity parameters (α_{xx}, α_{xy}, α_{yx}, and α_{yy}), which are mainly determined by the geometric symmetry and not very sensitive to wavelength and small structural fluctuations in such a subwavelength and nonresonant circumstance. The diffraction efficiency (the transmitted power divided by the power of hologram images,[45] which is directly related to the signal-to-noise ratio) of the metasurface is very high, with an average efficiency to 88% for the wavelength of 980 to 1400 nm (see Figure 2(c)). Thus, we do not need another pair of LP and QWP for cross-polarization analyses. The average optical efficiency (power of the letters divided by the total incident power) is calculated about 60%, which is not very high due to the low transmittance (68%). It can be enhanced through improving the fabrication technology to form smoother sample surfaces or by changing the material and working bandwidth to have lower absorption.

More importantly, this design can be utilized for independent control of two CP light phases. As illustrated in eq 1, ideally (a chiral meta-atom with subwavelength height), the phase response is opposite for scattered CP light as the helicity of incidence is swapped. In that situation, if the meta-device is designed to diffract to 30° for RCP light, it then will diffract to −30° for LCP light, which is similar to that based on PB phase, as shown in Figure S3. Notably, if such kind of dielectric meta-atoms shown in Figure 1(c) have wavelength-scale height, there may be other modes excited at the same time.[46] Contributions from other modes could all be attributed to the dynamic phase. Then, the phase response of such chiral meta-atom is no longer completely positive and negative related (see Figure S1(d)) but is still relevant (not the same) because the dynamic phase contributes almost equally to both RCP and LCP light. Then, the Jones matrix of such chiral meta-atoms under the circular base can be written as

https://dx.doi.org/10.1021/acs.nanolett.0c04902
Nano Lett. XXXX, XXX, XXX−XXX

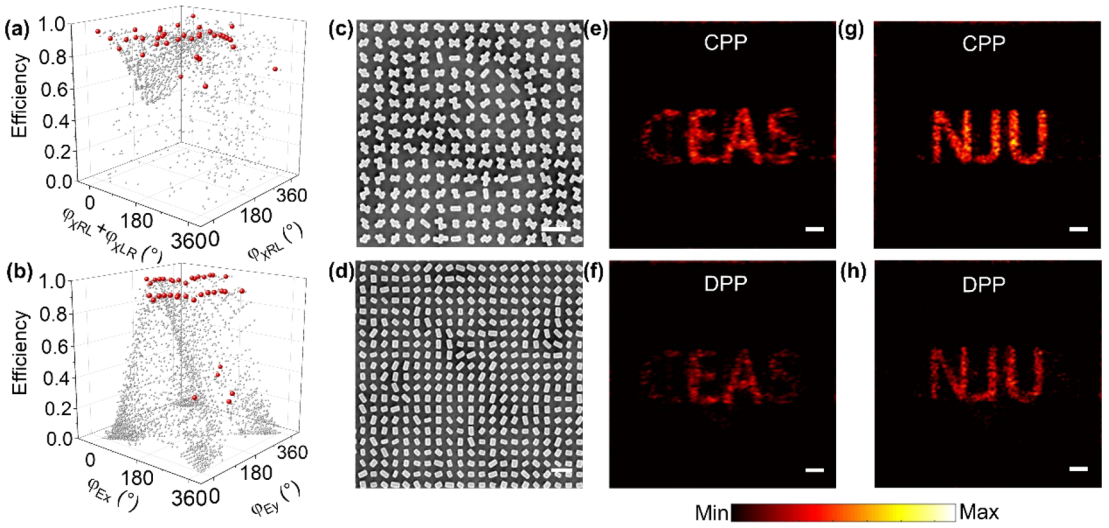

Figure 4. Spin-decoupled holograms with other methods of combing different principles. Simulated diffraction efficiency distribution with selected meta-atoms, which are marked in red for both the (a) CPP (chiral meta-atoms and PB phase) and (b) DPP (dynamic phase and PB phase) methods. SEM micrograph of the metasurface based on the (c) CPP and (d) DPP methods from a top view, where the scale bar is 1 μm. Experimental results with (e) RCP incidence and (g) LCP incidence based on the CPP method without analyzers, and corresponding results (f, h) based on the DPP method, where the scale bar is 20 μm.

$$J = \begin{bmatrix} e^{i\phi_{\chi}{}^{RR}} & e^{i\phi_{\chi}{}^{RL}} \\ e^{i\phi_{\chi}{}^{LR}} & e^{i\phi_{\chi}{}^{LL}} \end{bmatrix} \tag{2}$$

where $\varphi_{\chi LR}$ and $\varphi_{\chi RL}$ refers to the different phase delays of chiral meta-atoms for the working RCP light (LCP incidence) and LCP light (RCP incidence), respectively ($|\varphi_{\chi LR}| \neq |\varphi_{\chi RL}|$).

Hence, we are ready to access the spin-decoupled functions by carefully choosing the chiral meta-atoms, as exhibited in Figure 1(d). Figure 3(a) shows the phase delays ($\varphi_{\chi LR}$ and $\varphi_{\chi RL}$) and average efficiency distribution with different chiral meta-atoms. By choosing appropriate meta-atoms from the phase parameter space, the efficiency can be as high and uniform as possible. It is worth mentioning that avoidance of circular dichroism[47−49] could be helpful for the independent manipulation of CP light, both with high efficiencies. To avoid too many different meta-atoms, we only consider 8-grade phase control for one kind of spin light here, and then, the selected 64 kinds of meta-atoms with required phase delays and high efficiencies are marked in red balls. The specific parameters are listed in Table S2.

As a proof of concept, a spin-decoupled hologram metasurface is designed, fabricated, and demonstrated experimentally. For RCP incidence, the projected cross-CP hologram image is set as the four letters of "CEAS" (abbreviation of College of Engineering and Applied Sciences), while, for LCP light incidence, it is "NJU" at the same position. The SEM image of the fabricated metasurface (D = 250 μm) is shown in Figure 3(b), which also consisted of different Z-shaped chiral meta-atoms. Similarly, the difference between the actual (140 nm for the marked size) and the designed dimension (80 nm) proves its robustness as well. Different from the polarization multiplexed metasurfaces with interleaved meta-atoms,[22−28] here every single chiral meta-atom makes contributions to both types of scattered CP light. The transmitted intensity profiles under RCP and LCP light illumination without any analyzer in the projected plane are shown in Figures 3(c) and 3(d), respectively. Both examples of the imaging letters can be clearly identified, showing the capability of independent phase manipulation for the spin light. The hologram efficiency (the power of the letters divided by total transmitted light) is calculated as 74% and 81%, respectively. The total transmittance is measured about 52%, nearly the same as the metasurface designed for one CP light. Figure 3(e) and 3(f) illustrate the captured images at λ = 1200 nm, and the corresponding efficiencies are 75% and 89%, manifesting the broadband properties. Note that the degraded image quality in Figure 3(e, f) attributes to the inhomogeneous field intensity though it has comparable and even higher diffraction efficiencies than those in Figure 3(c, d). It is rightly due to the shift of the working wavelength away from the designed 980 nm. The homogeneity of field intensity is also an important factor in evaluating the image quality. In this regard, although our metasurface has a broadband property, its holography performances will decrease at other wavelengths.

Combining the phase response of chiral meta-atoms with PB phase (CPP), i.e., rotating the chiral meta-atoms, would also provide a novel method for independent manipulation of RCP light and LCP light. The Jones matrix here becomes

$$J = R_c(-\theta)\begin{bmatrix} e^{i\phi_{\chi}{}^{RR}} & e^{i\phi_{\chi}{}^{RL}} \\ e^{i\phi_{\chi}{}^{LR}} & e^{i\phi_{\chi}{}^{LL}} \end{bmatrix} R_c(\theta) = \begin{bmatrix} e^{i\phi_{\chi}{}^{RR}} & e^{i(2\theta+\phi_{\chi}{}^{RL})} \\ e^{i(-2\theta+\phi_{\chi}{}^{LR})} & e^{i\phi_{\chi}{}^{LL}} \end{bmatrix} \tag{3}$$

where $R_c(\theta) = \Lambda^{-1}R(\theta)\Lambda = \begin{bmatrix} \cos\theta - i\sin\theta & 0 \\ 0 & \cos\theta + i\sin\theta \end{bmatrix}$ is the rotation matrix in the circular base. The specific phase design principle is as follows:

$$\begin{aligned} \varphi_R(x, y) &= -\varphi_{PB}(x, y) + \varphi_{\chi}{}^{LR}(x, y) \\ \varphi_L(x, y) &= \varphi_{PB}(x, y) + \varphi_{\chi}{}^{RL}(x, y) \end{aligned} \tag{4}$$

where φ_R is the desired phase profile for the converted working RCP light and φ_L is the one for the LCP light. φ_{PB} is the contribution from the global meta-atoms rotation (2θ), opposite for CP light with different handedness.

https://dx.doi.org/10.1021/acs.nanolett.0c04902
Nano Lett. XXXX, XXX, XXX−XXX

A similar spin-decoupled hologram metasurface is designed to demonstrate the method experimentally. $\varphi_L(x,y)$ and $\varphi_R(x,y)$ are the calculated phase profiles for the hologram images ($\varphi_L(x,y)$ for "CEAS", $\varphi_R(x,y)$ for "NJU"). Substituting $\varphi_L(x,y)$ and $\varphi_R(x,y)$ into eq 4, one could obtain the required structural chiral phase and the PB phase distributions. Figure 4(a) exhibits that the simulated average efficiency (RCP and LCP) distribution in the parameter space consists of $\varphi_{\chi LR}(x,y)$ + $\varphi_{\chi RL}(x,y)$ and $\varphi_{\chi RL}(x,y)$ with selected meta-atoms marked in red (also listed in Table S3). Figure 4(c) shows the SEM image of the hologram metasurface (D = 250 μm). For RCP incidence, the total transmitted intensity profile in the projected plane is illustrated in Figure 4(e), where the four letters "CEAS" can be clearly recognized as well, indicating a high hologram efficiency of 83%. When the helicity of incidence is switched, the image swaps to "NJU" in the same position with nearly no crosstalk. The corresponding experimental result for LCP incidence is illustrated in Figure 4(g). The holography efficiency is calculated to be about 82%, almost equivalent to that of RCP incidence. Compared with the mechanism based on chiral meta-atoms without rotation, this method could reduce the number of meta-antennas with the same phase change order, while at the cost of the design complexity.

Another method utilizing different modulation principles, i.e., dynamic phase and PB phase, DPP[16,19,29−] is widely adopted for independent control of CP light. For comparison, a similar metasurface based on the DPP method was also designed and fabricated. The specific design principle can be found in Supporting Information Sec. VI. Figure 4(b) also illustrates the simulated efficiency distribution of the nanorods which have no planar chirality[50] in regards to the phase shifts. The meta-atoms with the highest efficiencies that meet the phase requirements (listed in Table S4) are selected and marked in red. However, it is still inevitable to choose the meta-atoms with lower efficiencies (the red ones in the lower area). Comparing Figure 4(a) with 4(b), it can be found that the total efficiency distribution based on the CPP method is much higher (with an average efficiency of 71%) and has better uniformity than that of the DPP method (with an average efficiency of 30%), due to wider parameter spaces. The SEM image of the metasurface based on the DPP method is shown in Figure 4(d), composed of different nanorods with different rotations. The corresponding experimental results are shown in Figure 4(f) and 4(h), with obviously lower intensity profiles than that based on the CPP method. The measured diffraction efficiencies based on the DPP method are 65% for CEAS and 71% for NJU, respectively, indicating results 10−20% lower than that based on the CPP method. As the semblable method of combining different principles, the better performances of the CPP method are attributed to the meta-atom efficiency advantages and fabrication robustness of the Z-shaped chiral meta-atoms. Our results evidently demonstrate the advantages of directly regulating CP light based on chiral meta-atoms.

In summary, we have demonstrated a new wavefront manipulation method based on chiral meta-atoms, which can be used to achieve the independent control of the CP light, as has been verified by spin-decoupled holograms with high performances. By combining the phase modulation of chiral meta-atoms and PB phase, the same functions can also be implemented with fewer types of meta-atoms. The compatibility indicates that chiral meta-atoms can be incorporated with other means to realize more complex functionalities. This work definitely enriches the working principle in metasurfaces design that is beneficial to further improve the performance of meta-devices and inspires new explorations in meta-design and applications.

■ ASSOCIATED CONTENT

Supporting Information

The Supporting Information is available free of charge at https://pubs.acs.org/doi/10.1021/acs.nanolett.0c04902.

Sample fabrication, derivation for electric-field response of meta-atoms, simulations of phase shifts of different kinds of meta-atoms, simulations of the symmetric response of chiral meta-atoms, and design principles of the spin-decoupled hologram based on the combination of dynamic phase and PB phase (PDF)

■ AUTHOR INFORMATION

Corresponding Author

Tao Li − *Nanjing University, National Laboratory of Solid State Microstructures, Key Laboratory of Intelligent Optical Sensing and Integration, Jiangsu Key Laboratory of Artificial Functional Materials, College of Engineering and Applied Sciences, Nanjing 210093, China; Collaborative Innovation Center of Advanced Microstructures, Nanjing 210093, China;* orcid.org/0000-0003-0049-471X; Email: taoli@nju.edu.cn

Authors

Chen Chen − *Nanjing University, National Laboratory of Solid State Microstructures, Key Laboratory of Intelligent Optical Sensing and Integration, Jiangsu Key Laboratory of Artificial Functional Materials, College of Engineering and Applied Sciences, Nanjing 210093, China; Collaborative Innovation Center of Advanced Microstructures, Nanjing 210093, China;* orcid.org/0000-0003-0599-0798

Shenglun Gao − *Nanjing University, National Laboratory of Solid State Microstructures, Key Laboratory of Intelligent Optical Sensing and Integration, Jiangsu Key Laboratory of Artificial Functional Materials, College of Engineering and Applied Sciences, Nanjing 210093, China; Collaborative Innovation Center of Advanced Microstructures, Nanjing 210093, China*

Wange Song − *Nanjing University, National Laboratory of Solid State Microstructures, Key Laboratory of Intelligent Optical Sensing and Integration, Jiangsu Key Laboratory of Artificial Functional Materials, College of Engineering and Applied Sciences, Nanjing 210093, China; Collaborative Innovation Center of Advanced Microstructures, Nanjing 210093, China;* orcid.org/0000-0001-8782-195X

Hanmeng Li − *Nanjing University, National Laboratory of Solid State Microstructures, Key Laboratory of Intelligent Optical Sensing and Integration, Jiangsu Key Laboratory of Artificial Functional Materials, College of Engineering and Applied Sciences, Nanjing 210093, China; Collaborative Innovation Center of Advanced Microstructures, Nanjing 210093, China*

Shi-Ning Zhu − *Nanjing University, National Laboratory of Solid State Microstructures, Key Laboratory of Intelligent Optical Sensing and Integration, Jiangsu Key Laboratory of Artificial Functional Materials, College of Engineering and Applied Sciences, Nanjing 210093, China; Collaborative*

https://dx.doi.org/10.1021/acs.nanolett.0c04902
Nano Lett. XXXX, XXX, XXX−XXX

Innovation Center of Advanced Microstructures, Nanjing 210093, China

Complete contact information is available at: https://pubs.acs.org/10.1021/acs.nanolett.0c04902

Author Contributions

T.L. and C.C. developed the idea. C.C. proposed the design and performed the numerical simulation. S.G. and H.L. fabricated the samples. C.C. performed the optical measurement with the help of W.S. T.L. supervised the project. C.C. and T.L. analyzed the results with help from all authors. All authors discussed the results. C.C. and T.L. wrote the manuscript with input from all authors.

Notes

The authors declare no competing financial interest.

■ ACKNOWLEDGMENTS

We acknowledge the microfabrication center of the National Laboratory of Solid State Microstructures (NLSSM) for technique support. This work was supported by the National Key R&D Program of China (2016YFA0202103, 2017YFA0303701) and the National Natural Science Foundation of China (91850204, 11674167). T.L. is thankful for the support from Dengfeng Project B of Nanjing University.

■ REFERENCES

(1) Yu, N.; Genevet, P.; Kats, M. A.; Aieta, F.; Tetienne, J. P.; Capasso, F.; Gaburro, Z. Light propagation with phase discontinuities: generalized laws of reflection and refraction. *Science* **2011**, *334* (6054), 333−337.

(2) Kildishev, A. V.; Boltasseva, A.; Shalaev, V. M. Planar photonics with metasurfaces. *Science* **2013**, *339* (6125), 1232009.

(3) Kamali, S. M.; Arbabi, E.; Arbabi, A.; Faraon, A. A review of dielectric optical metasurfaces for wavefront control. *Nanophotonics* **2018**, *7* (6), 1041−1068.

(4) Khorasaninejad, M.; Chen, W. T.; Devlin, R. C.; Oh, J.; Zhu, A. Y.; Capasso, F. Metalenses at visible wavelengths: Diffraction-limited focusing and subwavelength resolution imaging. *Science* **2016**, *352* (6290), 1190−1194.

(5) Wang, S.; Wu, P. C.; Su, V. C.; Lai, Y. C.; Chen, M. K.; Kuo, H. Y.; Chen, B. H.; Chen, Y. H.; Huang, T. T.; Wang, J. H.; Lin, R. M.; Kuan, C. H.; Li, T.; Wang, Z. L.; Zhu, S. N.; Tsai, D. P. A broadband achromatic metalens in the visible. *Nat. Nanotechnol.* **2018**, *13* (3), 227−232.

(6) Chen, C.; Song, W.; Chen, J. W.; Wang, J. H.; Chen, Y. H.; Xu, B.; Chen, M. K.; Li, H.; Fang, B.; Chen, J.; Kuo, H. Y.; Wang, S.; Tsai, D. P.; Li, T.; Zhu, S. Spectral tomographic imaging with aplanatic metalens. *Light: Sci. Appl.* **2019**, *8* (1), 1−8.

(7) Chen, W. T.; Yang, K. Y.; Wang, C. M.; Huang, Y. W.; Sun, G.; Chiang, I. D.; Liao, C.; Hsu, W.; Lin, H.; Sun, S.; Zhou, L.; Liu, A.; Tsai, D. P. High-efficiency broadband meta-hologram with polarization-controlled dual images. *Nano Lett.* **2014**, *14* (1), 225−230.

(8) Li, X.; Chen, L.; Li, Y.; Zhang, X.; Pu, M.; Zhao, Z.; Ma, X.; Wang, Y.; Hong, M.; Luo, X. Multicolor 3D meta-holography by broadband plasmonic modulation. *Sci. Adv.* **2016**, *2*, e1601102.

(9) Huang, L.; Zhang, S.; Zentgraf, T. Metasurface holography: from fundamentals to applications. *Nanophotonics* **2018**, *7*, 1169−1190.

(10) Ding, F.; Wang, Z.; He, S.; Shalaev, V. M.; Kildishev, A. V. Broadband high-efficiency half-wave plate: a supercell-based plasmonic metasurface approach. *ACS Nano* **2015**, *9* (4), 4111−4119.

(11) Yu, N.; Aieta, F.; Genevet, P.; Kats, M. A.; Gaburro, Z.; Capasso, F. A broadband, background-free quarter-wave plate based on plasmonic metasurfaces. *Nano Lett.* **2012**, *12* (12), 6328−6333.

(12) Sun, S.; Yang, K. Y.; Wang, C. M.; Juan, T. K.; Chen, W. T.; Liao, C. Y.; He, Q.; Xiao, S.; Kung, W.-T.; Guo, G.-Y.; Zhou, L.; Tsai, D. P. High-efficiency broadband anomalous reflection by gradient meta-surfaces. *Nano Lett.* **2012**, *12* (12), 6223−6229.

(13) Sun, S.; He, Q.; Xiao, S.; Xu, Q.; Li, X.; Zhou, L. Gradient-index meta-surfaces as a bridge linking propagating waves and surface waves. *Nat. Mater.* **2012**, *11* (5), 426−431.

(14) Decker, M.; Staude, I.; Falkner, M.; Dominguez, J.; Neshev, D. N.; Brener, I.; Pertsch, T.; Kivshar, Y. S. High-efficiency dielectric Huygens' surfaces. *Adv. Opt. Mater.* **2015**, *3* (6), 813−820.

(15) Huang, L.; Chen, X.; Mühlenbernd, H.; Li, G.; Bai, B.; Tan, Q.; Jin, G.; Zentgraf, T.; Zhang, S. Dispersionless phase discontinuities for controlling light propagation. *Nano Lett.* **2012**, *12* (11), 5750−5755.

(16) Arbabi, A.; Horie, Y.; Bagheri, M.; Faraon, A. Dielectric metasurfaces for complete control of phase and polarization with subwavelength spatial resolution and high transmission. *Nat. Nanotechnol.* **2015**, *10* (11), 937−943.

(17) Hsiao, H.-H.; Chu, C. H.; Tsai, D. P. Fundamentals and Applications of Metasurfaces. *Small Meth.* **2017**, *1*, 1600064.

(18) Wang, S.; Wu, P. C.; Su, V.-C.; Lai, Y.-C.; Hung Chu, C.; Chen, J.-W.; Lu, S.-H.; Chen, J.; Xu, B.; Kuan, C.-H.; Li, T.; Zhu, S.; Tsai, D. P. Broadband achromatic optical metasurface devices. *Nat. Commun.* **2017**, *8* (1), 1−9.

(19) Balthasar Mueller, J. P.; Rubin, N. A.; Devlin, R. C.; Groever, B.; Capasso, F. Metasurface polarization optics: independent phase control of arbitrary orthogonal states of polarization. *Phys. Rev. Lett.* **2017**, *118* (11), 113901.

(20) Bai, G. D.; Ma, Q.; Li, R. Q.; Mu, J.; Jing, H. B.; Zhang, L.; Cui, T. J. Spin-Symmetry Breaking Through Metasurface Geometric Phases. *Phys. Rev. Appl.* **2019**, *12* (4), 044042.

(21) Li, Z.; Kim, I.; Zhang, L.; Mehmood, M. Q.; Anwar, M. S.; Saleem, M.; Lee, D.; Nam, K. T.; Zhang, S.; Luk'yanchuk, B.; Wang, Y.; Zheng, G.; Rho, J.; Qiu, C.-W. Dielectric meta-holograms enabled with dual magnetic resonances in visible light. *ACS Nano* **2017**, *11* (9), 9382−9389.

(22) Wen, D.; Yue, F.; Li, G.; Zheng, G.; Chan, K.; Chen, S.; Chen, M.; Li, K. F.; Wong, P. W. H.; Cheah, K. W.; Yue Bun Pun, E.; Zhang, S.; Chen, X. Helicity multiplexed broadband metasurface holograms. *Nat. Commun.* **2015**, *6* (1), 1−7.

(23) Wang, Q.; Plum, E.; Yang, Q.; Zhang, X.; Xu, Q.; Xu, Y.; Han, J.; Zhang, W. Reflective chiral meta-holography: multiplexing holograms for circularly polarized waves. *Light: Sci. Appl.* **2018**, *7* (1), 1−9.

(24) Zhang, X.; Yang, S.; Yue, W.; Xu, Q.; Tian, C.; Zhang, X.; Plum, E.; Zhang, S.; Han, J.; Zhang, W. Direct polarization measurement using a multiplexed Pancharatnam−Berry metahologram. *Optica* **2019**, *6* (9), 1190−1198.

(25) Chen, Y.; Yang, X.; Gao, J. Spin-controlled wavefront shaping with plasmonic chiral geometric metasurfaces. *Light: Sci. Appl.* **2018**, *7* (1), 1−10.

(26) Mehmood, M. Q.; Mei, S.; Hussain, S.; Huang, K.; Siew, S. Y.; Zhang, L.; Zhang, T.; Ling, X.; Liu, H.; Teng, J.; Danner, A.; Zhang, S.; Qiu, C. Visible-frequency metasurface for structuring and spatially multiplexing optical vortices. *Adv. Mater.* **2016**, *28* (13), 2533−2539.

(27) Wen, D.; Chen, S.; Yue, F.; Chan, K.; Chen, M.; Ardron, M.; Li, K.; Wong, P. W. H.; Cheah, K. W.; Pun, E. Y. B.; Li, G.; Zhang, S.; Chen, X. Metasurface device with helicity-dependent functionality. *Adv. Opt. Mater.* **2016**, *4* (2), 321−327.

(28) Khorasaninejad, M.; Ambrosio, A.; Kanhaiya, P.; Capasso, F. Broadband and chiral binary dielectric meta-holograms. *Sci. Adv.* **2016**, *2* (5), e1501258.

(29) Devlin, R. C.; Ambrosio, A.; Rubin, N. A.; Mueller, J. B.; Capasso, F. Arbitrary spin-to−orbital angular momentum conversion of light. *Science* **2017**, *358* (6365), 896−901.

(30) Xu, H. X.; Han, L.; Li, Y.; Sun, Y.; Zhao, J.; Zhang, S.; Qiu, C. W. Completely spin-decoupled dual-phase hybrid metasurfaces for arbitrary wavefront control. *ACS Photonics* **2019**, *6* (1), 211−220.

(31) Ding, G.; Chen, K.; Luo, X.; Zhao, J.; Jiang, T.; Feng, Y. Dual-helicity decoupled coding metasurface for independent spin-to-orbital angular momentum conversion. *Phys. Rev. Appl.* **2019**, *11* (4), 044043.

(32) Fan, Q.; Zhu, W.; Liang, Y.; Huo, P.; Zhang, C.; Agrawal, A.; Huang, K.; Luo, X.; Lu, Y.; Qiu, C.; Lezec, H. J.; Xu, T. Broadband generation of photonic spin-controlled arbitrary accelerating light beams in the visible. *Nano Lett.* **2019**, *19* (2), 1158−1165.
(33) Rubin, N. A.; D'Aversa, G.; Chevalier, P.; Shi, Z.; Chen, W. T.; Capasso, F. Matrix Fourier optics enables a compact full-Stokes polarization camera. *Science* **2019**, *365* (6448), eaax1839.
(34) Li, S.; Li, X.; Wang, G.; Liu, S.; Zhang, L.; Zeng, C.; Wang, L.; Sun, Q.; Zhao, W.; Zhang, W. Multidimensional Manipulation of Photonic Spin Hall Effect with a Single-Layer Dielectric Metasurface. *Adv. Opt. Mater.* **2019**, *7* (5), 1801365.
(35) Ding, G.; Chen, K.; Qian, G.; Zhao, J.; Jiang, T.; Feng, Y.; Wang, Z. Independent Energy Allocation of Dual-Helical Multi-Beams with Spin-Selective Transmissive Metasurface. *Adv. Opt. Mater.* **2020**, *8* (16), 2000342.
(36) Zhang, F.; Pu, M.; Luo, J.; Yu, H.; Luo, X. Symmetry breaking of photonic spin-orbit interactions in metasurfaces. *Opto-Elec. Eng.* **2017**, *44* (3), 319−325.
(37) Bai, G. D.; Ma, Q.; Li, R. Q.; Mu, J.; Jing, H. B.; Zhang, L.; Cui, T. J. Spin-Symmetry Breaking Through Metasurface Geometric Phases. *Phys. Rev. Appl.* **2019**, *12* (4), 044042.
(38) Yuan, Y.; Zhang, K.; Ratni, B.; Song, Q.; Ding, X.; Wu, Q.; Burokur, S. N.; Genevet, P. Independent phase modulation for quadruplex polarization channels enabled by chirality-assisted geometric-phase metasurfaces. *Nat. Commun.* **2020**, *11* (1), 1−9.
(39) Guo, Y.; Pu, M.; Zhao, Z.; Wang, Y.; Jin, J.; Gao, P.; Li, X.; Ma, X.; Luo, X. Merging geometric phase and plasmon retardation phase in continuously shaped metasurfaces for arbitrary orbital angular momentum generation. *ACS Photonics* **2016**, *3*, 2022.
(40) Zhang, F.; Pu, M.; Li, X.; Gao, P.; Ma, X.; Luo, J.; Yu, H.; Luo, X. All-dielectric metasurfaces for simultaneous giant circular asymmetric transmission and wavefront shaping based on asymmetric photonic spin-orbit interactions. *Adv. Funct. Mater.* **2017**, *27*, 1704295.
(41) Wang, Z.; Jia, H.; Yao, K.; Cai, W.; Chen, H.; Liu, Y. Circular dichroism metamirrors with near-perfect extinction. *ACS Photonics* **2016**, *3* (11), 2096−2101.
(42) Kamali, S. M.; Arbabi, E.; Arbabi, A.; Horie, Y.; Faraon, A. Highly tunable elastic dielectric metasurface lenses. *Laser Photon. Rev.* **2016**, *10* (6), 1002−1008.
(43) Gerchberg, R. W.; Saxton, W. O. A practical algorithm for the determination of phase from image and diffraction plane pictures. *Optik* **1972**, *35*, 227−246.
(44) Fienup, J. R. Phase retrieval algorithms: a comparison. *Appl. Opt.* **1982**, *21* (15), 2758−2769.
(45) Wang, L.; Kruk, S.; Tang, H.; Li, T.; Kravchenko, I.; Neshev, D. N.; Kivshar, Y. S. Grayscale transparent metasurface holograms. *Optica* **2016**, *3* (12), 1504−1505.
(46) Kamali, S. M.; Arbabi, A.; Arbabi, E.; Horie, Y.; Faraon, A. Decoupling optical function and geometrical form using conformal flexible dielectric metasurfaces. *Nat. Commun.* **2017**, *7* (1), 1−7.
(47) Ma, Z.; Li, Y.; Li, Y.; Gong, Y.; Maier, S. A.; Hong, M. All-dielectric planar chiral metasurface with gradient geometric phase. *Opt. Express* **2018**, *26* (5), 6067−6078.
(48) Fedotov, V. A.; Mladyonov, P. L.; Prosvirnin, S. L.; Rogacheva, A. V.; Chen, Y.; Zheludev, N. I. Asymmetric propagation of electromagnetic waves through a planar chiral structure. *Phys. Rev. Lett.* **2006**, *97* (16), 167401.
(49) Li, W.; Coppens, Z. J.; Besteiro, L. V.; Wang, W.; Govorov, A. O.; Valentine, J. Circularly polarized light detection with hot electrons in chiral plasmonic metamaterials. *Nat. Commun.* **2015**, *6* (1), 1−7.
(50) Wang, Z.; Cheng, F.; Winsor, T.; Liu, Y. Optical chiral metamaterials: a review of the fundamentals, fabrication methods and applications. *Nanotechnology* **2016**, *27* (41), 412001.

https://dx.doi.org/10.1021/acs.nanolett.0c04902
Nano Lett. XXXX, XXX, XXX−XXX